Presented at the IEEE Nuclear Science
Symposium, San Francisco, CA,
November 19 - 21, 1975

LBL-3872
c.1

AXIAL TOMOGRAPHY AND THREE DIMENSIONAL IMAGE RECONSTRUCTION

L. T. Chang, B. Macdonald, and V. Perez-Mendez

November 1975

Prepared for the U. S. Energy Research and
Development Administration under Contract W-7405-ENG-48

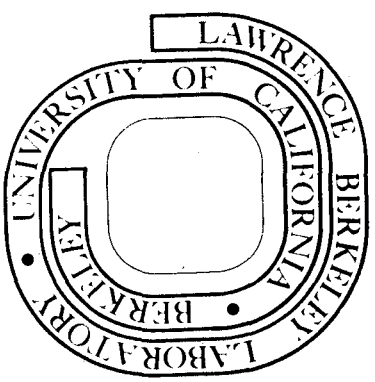

LBL-3872
c.1

DISCLAIMER

AXIAL TOMOGRAPHY AND THREE DIMENSIONAL IMAGE RECONSTRUCTION

L.T. Chang, B. Macdonald, and V. Perez-Mendez

Lawrence Berkeley Laboratory
University of California
Berkeley, California

Summary

A number of existing cameras for Nuclear Medicine imaging of radio-isotope distributions give depth information about the distribution. These devices have in common that they provide tomographic images of the object, that is, that images of a given object plane have that plane in focus and all other object planes contribute an out-of-focus background superimposed on the in-focus image.

We present here a method for three dimensional reconstruction of these axial tomographic images which removes the blurred off-plane activity from a number of transverse planes simultaneously. The method is applicable to a number of tomographic cameras, such as the multiple single-pinhole camera, the rotating slanted-hole collimator, the Anger focussing tomographic scanner, and the positron camera. The method can be implemented on a small computer having a disc system.

Introduction

A number of cameras for Nuclear Medicine imaging have been built in the recent past which provide depth information about radio-isotope distributions instead of the simple projected views produced by pinhole collimators. These devices gave images which were, in principle, similar to the tomographic images given by a microscope- any given plane was in focus while the out-of-focus planes gave only a smoothed-out background. In microscopy, object contrast and resolution are high and the out-of-focus background is not disturbing. In Nuclear Medicine imaging with its low resolution and its frequently low contrast objects it is often not possible to distinguish the in-focus plane from the out-of-focus images. Removal of the background would enable detection of smaller lesions and of lesions of lower contrast.

The method of three dimensional imaging we present here removes this blurred background from a number of parallel planes through the object simultaneously. It is applicable to a number of existing tomographic cameras and we discuss three of these cameras below. Data taken by such a camera provides information from which a computer can produce tomographic images on transverse planes through the object. Using these tomograms and a knowledge of the geometric imaging properties of the device, reconstructions of the original object are made on these planes with a deconvolution technique.

Forming the Tomographic Images

Imaging devices which give depth information about a source point require radiation from the point to be detected from distinctly separate directions. In Nuclear Medicine imaging devices the direction of each gamma ray event is known and, if separate views of a source distribution have been made, a tomographic image on any plane through the source can be made by back-projecting the gamma rays onto that plane.

* This work has been supported by the U.S. Atomic Energy Commission and by the National Institute of General Medical Services of the National Institutes of Health, Fellowship #1F03GM57292-01, and Grant #GM21017.

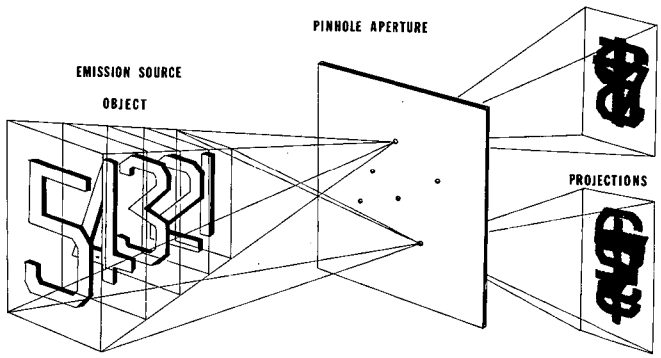

Fig. 1 Making the different views with the multiple single-pinhole camera

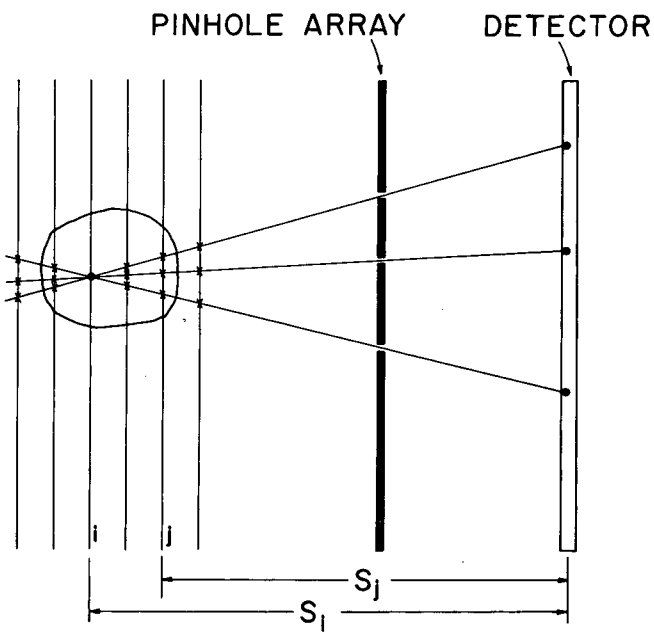

Fig. 2 Multiple Single-Pinhole Camera- Response to a point source. The tomographic images of the point are shown as the sum of back projections of the single-pinhole views.

Multiple Single Pinhole Camera

One such tomographic device uses multiple single-pinhole views (Fig. 1). The depth-information properties of these multiple views is illustrated in Fig. 2 where the source distribution is a single point. An exposure is made using one pinhole selected from the array. Tomographic images on a number of planes are made by back projecting photons from this exposure through the same pinhole and adding the appropriate intensity to each tomographic plane at its intersection with the line. The process is repeated for the other views and the final tomographic plane

image is the sum of contributions from all these views. The plane which actually contained the point source has a sharp image while in other planes the image of the point source is blurred out.

In analyzing image formation it is useful to use the point response function $h_{ij}(\underline{r},\underline{r}')$. This function, characteristic of the imaging device used, describes the response at point $\underline{r}$ in plane j to a point source at point $\underline{r}'$ in plane i. From Fig. 2 it is seen that this function, or blurring pattern, for the multiple single-pinhole camera has a shape similar to the original array of pinholes but with a size which depends upon the geometry. Fig. 3a shows one of the pinhole arrays used in our work.

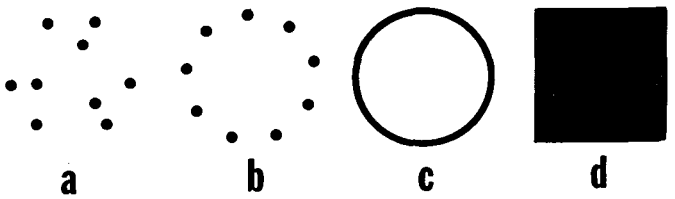

Fig. 3 Blurring Patterns - a) For multiple pinhole array. b) For rotating slanted-hole collimator with discrete rotations. c) For rotating slanted-hole collimator with continuous rotation. d) For positron camera with data selection.

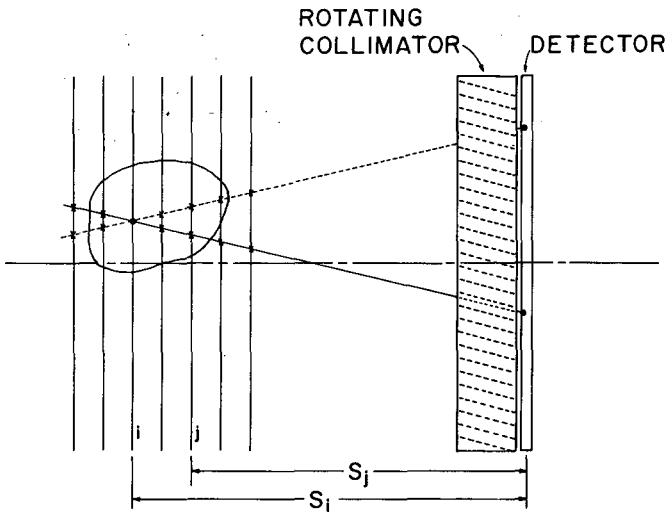

Fig. 4 Rotating Slanted-Hole Collimator Camera- Response to a point source. The tomographic images of the point are shown for two positions of the collimator, 0^o and 180^o.

Rotating Slanted-hole Collimator Camera

Another device used to obtain tomographic images in Nuclear Medicine is the rotating slanted-hole collimator (Fig. 4). The collimator rotates about an axis perpendicular to the detector and the parallel holes are slanted at an angle to this axis, generally about 20 degrees. When the collimator is at a given position the image of a point source is a single point on the detector. When the collimator has rotated 180^o the image of this point source has traveled on the arc of a circle to an opposite position. As done previously, tomographic images on a number of transverse planes can be made by back projecting the detector image obtained at a given position of the collimator along the known direction of the parallel holes and then repeating this process for all positions of the collimator.

In one mode of operation of this camera views are taken at discrete positions of the collimator and the blurring patterns have a shape similar to Fig. 3b.[1]

In another mode the collimator is rotated continuously during data collection and the blurring pattern is a circle (Fig. 3c).[2]

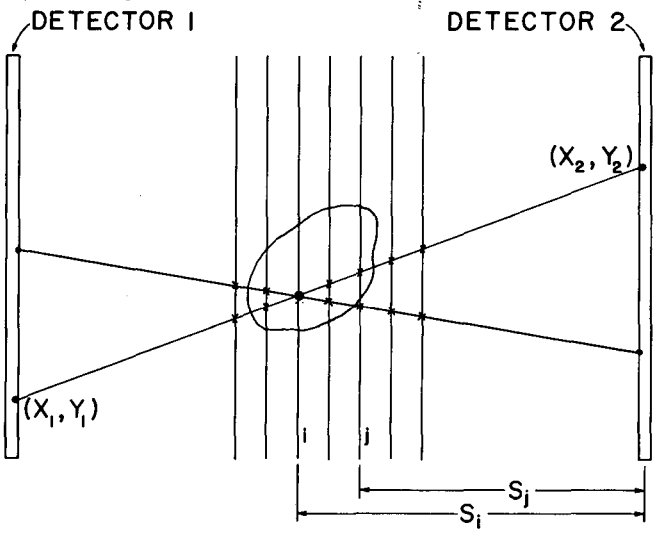

Fig. 5 Positron Camera- Response to a point source. The tomographic images of the point are shown for two positron events.

Positron Camera

Positron cameras are currently under intensive development[3] because of their ability to give tomographic images without the use of a collimator and the associated loss of intensity. The two 511 KeV annihilation gamma-rays from a positron source radiate from the source point at 180^o to each other (Fig. 5). Interactions with two detectors determine, as in the previous cases, only a line on which the source lies. Projection of events detected onto a transverse plane gives, again, a tomographic image of the source distribution with that plane in focus and other planes blurred and superimposed.

The fraction of detected events from a point source in the midplane, say, decreases considerably as the point source moves away from the center of the plane. Our three dimensional image reconstruction method requires that the point response function remains constant in shape, size, and intensity as the point source moves over the camera field of view on a given plane, although it may be different for different planes. This blurring pattern can be maintained constant over a given area of a plane if the computer which constructs the tomographic image planes accepts data only for those events for which $|x_2-x_1| \leq d$ and $|y_2-y_1| \leq d$ where d is smaller than W, the width of the detectors. The region of constant detection efficiency for the midplane which results is a square of width W-d. The blurring pattern is also a square (Fig. 3d).

Object Reconstruction from Tomographic Images

Each tomographic image plane of a three dimensional object has a finite width slab of the object in focus. The thickness of this slab, the depth of field of the camera, depends only on geometry and detector resolution. Of course, included in the tomographic image, superimposed on the in-focus object plane, are the blurred contributions from all the other planes which we are trying to eliminate in the deconvolution method outlined below. The resulting image of the object will be a series of images on adjacent planes, each representing the object averaged over the depth of field of the imaging system. Lateral and depth resolutions after deconvolution are the same as before. We are only removing the off-plane contributions and not looking for super-

resolution.

We assume in the following that the object is located in N_p planes and is represented by the functions $o_i(\underline{r})$, $i=1,\ldots N_p$. N_p tomograms $t_j(\underline{r})$ are formed by a computer from camera data using the back projection methods discussed previously. Since the blurring function $h_{ij}(\underline{r},\underline{r}')$ represents the system response at $\underline{r}$ on plane j due to a point source of unit intensity at $\underline{r}'$ on plane i, the total contribution from plane i to plane j is just $\int o_i(\underline{r}')h_{ij}(\underline{r},\underline{r}')d^2\underline{r}'$. Since the tomographic image has contributions from all object planes we have

$$t_j(\underline{r}) = \sum_{i=1}^{N_p} \int o_i(\underline{r}')\, h_{ij}(\underline{r},\underline{r}')\, d^2\underline{r}' \qquad j=1,\ldots N_p \quad (1)$$

Multiple Single Pinhole Camera

Fig. 2 shows that h_{ii} is a delta function of intensity N_h and the $h_{ij}(\underline{r},\underline{r}')$ is just the pattern h of the N_h hole array used, but displaced and with a size dependent on geometry. If $m_{ij} \equiv (S_i-S_j)/S_i$ is the size parameter and the pinholes in h are located at positions $\underline{r}_k$, $k=1,\ldots N_h$, we have

$$h_{ij}(\underline{r},\underline{r}') = h(\underline{r}-\underline{r}'S_j/S_i,\, m_{ij}) \qquad i,j=1,\ldots N_p \quad (2)$$
$$= \sum_k \delta(\underline{r} - (\underline{r}'S_j/S_i + m_{ij}\underline{r}_k))$$

Using this in Eq. (1) we have

$$t_j(\underline{r}) = \sum (S_i/S_j)^2 \int o_i(\underline{r}''S_i/S_j)\, h(\underline{r}-\underline{r}'', m_{ij})\, d^2\underline{r}''$$
$$= \sum_{i=1}^{N_p} (S_i/S_j)^2 \; o_i(\underline{r}S_i/S_j) * h(\underline{r}, m_{ij}) \qquad (3)$$

For a given value of $\underline{r}$, position relative to the optic axis, equation (2) is a set of N_p equations in the N_p variables o_i. The t_j's are combinations of single pinhole image data and $h(\underline{r},m_{ij})$ depends only on the pinhole locations in the array and the placement of the reconstruction planes.

Taking the Fourier transform of Eq. (2) and using the similarity theorem for Fourier transforms gives

$$T_j(\underline{u}) = \sum_{i=1}^{N_p} O_i(\underline{u}S_j/S_i)\, H_{ij}(\underline{u}) \qquad j=1,\ldots N_p \qquad (4)$$

where the quantities T_j, O_i, H_{ij}, Fourier transforms of the corresponding quantities of Eq.(2), are functions of the spatial frequency $\underline{u}$. To eliminate the j-dependence of the quantities O_i we let $\underline{u} = \underline{u}'/S_j$

$$T_j(\underline{u}'/S_j) = \sum_{i=1}^{N_p} O_i(\underline{u}'/S_i)\, H_{ij}(\underline{u}'/S_j) \quad j=1,\ldots N_p \quad (5)$$

For those (angular) spatial frequencies $\underline{u}'$ for which the determinant $D(\underline{u}') \equiv |H_{ij}(\underline{u}'/S_j)|$ is not zero, Eqs. (5) can be solved for $O_i(\underline{u}'/S_i)$ and inverse Fourier transforms give the desired background-free images $o_i(\underline{r})$.

We note that h in Eq.3 depends only on the difference, $\underline{r}-\underline{r}''$, of response point and source point locations. The more general functional dependence $h_{ij}(\underline{r},\underline{r}')$ makes the integral equation (1) much more difficult to solve.

Determinant - When the determinant $D(\underline{u}')$ equals zero for some (angular) spatial frequency $\underline{u}'$, this component cannot be determined for any object plane. Using the analytic form of the Fourier transform of the delta-function pinholes of Eq. 2 we can investigate the properties of the determinant

$$H_{ij}(\underline{u}'/S_j) = \sum_{k=1}^{N_h} e^{-i2\pi \underline{u}'\cdot\underline{r}_k\,[(S_i-S_j)/S_iS_j]} \qquad i,j=1,\ldots N_p \qquad (6)$$

At zero spatial frequency $H_{ij}(o) = N_h$ and the $N_p \times N_p$ determinant D(o) is identically zero. This means that our reconstructions $o_i(\underline{r})$ are indefinite by an additive constant. This is not a problem if this is the only zero since this constant can be determined by a subsidiary condition, for instance, that $o_i(\underline{r})$ has no negative value. The general property, $D(0) = 0$, arises from the fact that only a projection at 90° will give the total intensity of an object plane. All other projections for an object which has, say, N_p planes of uniform intensity ($o_i(\underline{r})=I_i$) give the same value (ΣI_i) and assignment of a given plane's intensity is not possible.

Because the slope of D(u) is also zero at u=o, the determinant has small values near the origin, for instance, at the first harmonic of spatial frequency, u_1. Since the reconstruction $O_k(u_1)$ has terms in it proportional to $T_j(u_1)/D(u_1)$, when $D(u_1)$ is small $T_j(u_1)$ must be correspondingly small so as to give the correct value for $O_k(u_1)$. $T_j(u_1)$ depends on data from the camera and therefore has statistical fluctuations in it which are magnified by $1/D(u_1)$, giving rise to incorrect values for $O_k(u_1)$. These low frequency fluctuations have not been a problem so far for up to five-plane reconstructions but they may turn out to be a limitation of the reconstruction method.

Other zeroes of the determinant can easily be avoided by choice of a suitable pinhole array. The determinant for various arrays is shown in Fig. 6 as a function of (vector) spatial frequency and also plotted in Fig. 7 as a function of u_x. It is seen that a regularly spaced array has numerous zeroes in the frequency plane while other, non-regular arrays do not have this problem.

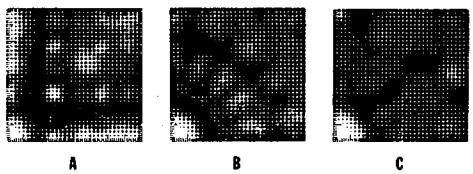

Fig. 6 The determinant $D(\underline{u}')$ of the reconstruction matrix for three planes for the multiple single-pinhole camera. a) For a 3 x 3 regular pinhole array. b) For the pinhole array of Fig. 2b. c) For the pinhole array of Fig. 2a.

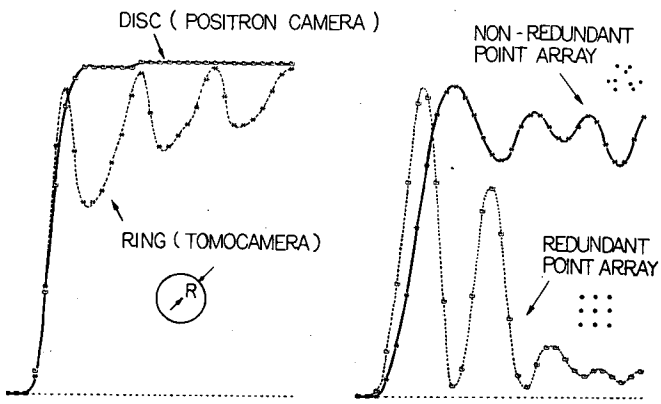

Fig. 7. Determinant of the reconstruction matrix as a function of spatial frequency for different cameras and blurring patterns.

Reconstructions - To investigate the reconstruction method a computer simulation was made of an object in three planes (Fig. 8). The tomographic images of Fig. 8c were done using the pinhole array of Fig. 3a. It is seen that t_3, for example, has o_3 in focus with blurred contributions from the other planes. Using these images the reconstructions of Fig. 8d were made, in excellent agreement with the original. However, these tomograms were produced as if the

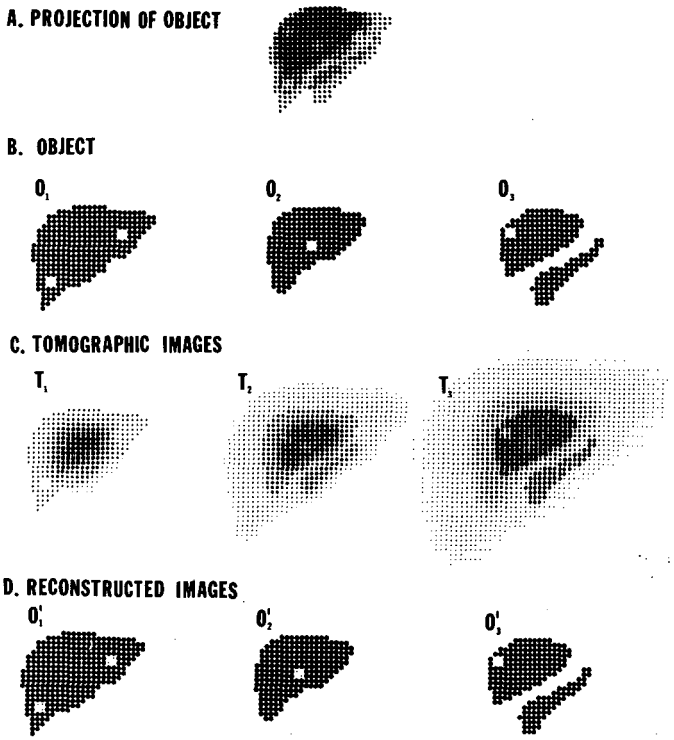

Fig. 8. Image Reconstruction with multiple single-pinhole views- Computer simulation assuming no statistical variation of object picture element intensities between views. a) Projected view of object as it would be seen with a parallel-hole collimator. b) The three dimensional object located in three planes. c) Tomographic images constructed using nine pinholes with the blurring pattern of Fig. 2a. d) Reconstruction of the object using the tomographic images t_1,t_2,t_3.

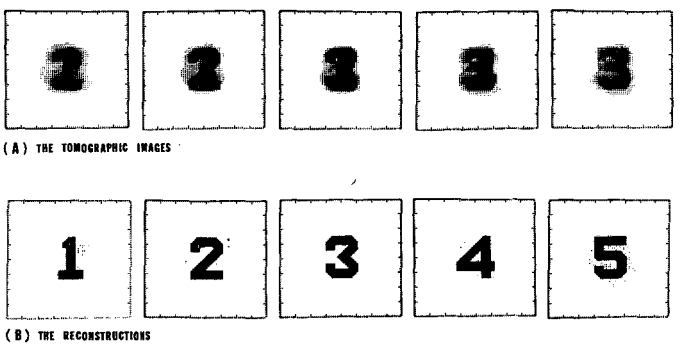

Fig. 9. Image Reconstruction- Computer simulation assuming 5% statistical variation of object picture elements. a) Tomographic images on the five planes of a five plane object using blurring pattern of Fig. 2a. b) Reconstructions of these planes showing a small amount of background introduced by photon statistics.

detector had collected an infinite number of photons from each picture element. A more realistic case is given in Fig. 9. Here, an average of 400 counts total was assumed to have been collected from each picture element of a five-plane object. These 400 counts, however, were distributed statistically among the 9 pinhole views and the tomograms of Fig.9a were then formed. The reconstructions show excellent agreement with the originals but a small background can be seen.

A radioactive source was used with a xenon-filled multiwire proportional chamber (48cm square, 2mm resolution) and the digitized gamma-event coordinates were put on magnetic tape for input to the reconstruction program. The object, a circle, cross, and triangle, was located on three planes, S_1=20cm, S_2=25cm, S_3=30cm. Detector to pinhole array distance was 39cm. The pinhole array of Fig. 3b (4mm holes 9cm diameter) was used so as to maximize depth resolution for a given field of view. The tomograms and their reconstructions are shown in Fig. 10. Because of the high object contrast, not usually the case in Nuclear Medicine, the nature of the objects can be inferred from the tomograms alone. The reconstruction method, however, has clearly successfully removed artifacts and background from the tomograms.

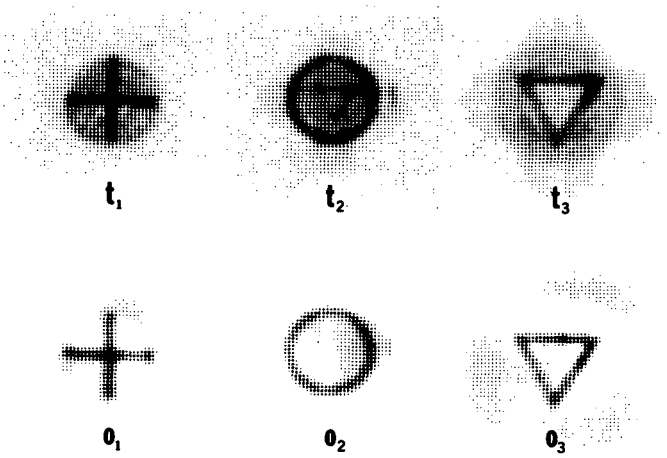

Fig. 10. Tomograms (t_1,t_2,t_3) and their reconstructions (o_1,o_2,o_3) using a wire proportional chamber and the pinhole array of Fig. 2a.

The Rotating Slanted-Hole Collimator

For this camera, and also for the positron camera, the point response function has the form (analogous to Eq. 2)

$$h_{ij}(\underline{r},\underline{r}') = h(\underline{r}-\underline{r}', m_{ij}) \qquad (7)$$

where the size parameter $m_{ij} = (S_i-S_j)\tan\alpha$, and α is the angle the slanted holes make with the collimator's axis of rotation. The absence of the coefficient S_j/S_i which multiplies $\underline{r}'$ in the multiple pinhole case makes the reconstruction equations (analogous to Eq. 5) much simpler -

$$T_j(\underline{u}) = \sum_{i=1}^{N_p} O_i(\underline{u})\, H_{ij}(\underline{u}) \qquad j=1,\ldots N_p \qquad (8)$$

We note there are no scale changes required here.

When this camera is operated in the continuously rotating mode the blur pattern is an annulus (Fig.3c) and H_{ij} depends on the magnitude of spatial frequency, u, and not on its vector components. $H_{ij}(u)$ is a matrix symmetric in the indices i and j. In this mode we have

$$H_{ij}(u) = J_o(m_{ij}u) \qquad (9)$$

where J_o is the Bessel function of order zero. The determinant of this matrix for four regularly space planes is shown in Fig. 7.

The Positron Camera

As discussed before, data from the positron camera should be taken with some maximum allowable difference in the coordinate values, $d = \max(|x_1-x_2|) = \max(|y_1-y_2|)$ (Fig. 5). When this is done, in each plane which is sufficiently near the midplane there is an area where point sources are detected with constant efficiency. The point response function is then given by Eq. 7 where tan α in m_{ij} is d/(chamber separation). The equations governing tomogram formation are the same as Eqs. (8) and the reconstructed object's Fourier transform is given by

$$O_k(\underline{u}) = \sum_{j=1}^{N_p} G_{jk}(\underline{u})\, T_j(\underline{u}) \qquad k=1,\ldots N_p \tag{10}$$

where the $N_p x N_p$ matrix $G(\underline{u})$ is the inverse of $H(\underline{u})$ evaluated at the spatial frequency $\underline{u}$.

If the point response function is evaluated for small angles α (neglecting solid angle effects) we have

$$H_{ij}(\underline{u}) = \left[\sin(a_{ij}u_x)/(a_{ij}u_x)\right]\left[\sin(a_{ij}u_y)/(a_{ij}u_y)\right] \tag{11}$$

and $a_{ij} = 2\pi(S_i-S_j)\tan\alpha$. A graph of the determinant $|H_{ij}(\underline{u})|$ is given in Fig. 10a and shows the familiar property of being zero at $\underline{u}=0$. The determinant for the positron camera, however, is the only one of the cameras studied which does not show a decrease at higher spatial frequencies which may give the positron camera somewhat better noise characteristics. Usually, these cameras are constructed to accept a large solid angle ($\alpha = \sim 40^\circ$) and the effects of solid angle must be put into the point response functions.

In general, $H_{ij}(\underline{u})$ is real, symmetric in i and j, and is also a separable function of u_x and u_y because the blurring pattern is a square. When the tomographic planes are regularly spaced $H_{ij}(\underline{u})$ depends on the difference $|i-j|$ so that, out of the N_p^2 elements of the matrix H (for each spatial frequency component), there are only (N_p-1) different values. The inverse matrix G is, of course, also real and symmetric but it is not separable. For regularly spaced planes it has about $(N_p/2 + 1)^2$ different elements for each spatial frequency component.

Computational Requirements- Operation of this reconstruction method will require only the use of a small computer together with an associated disc system, and work is in progress to implement this. A random access memory of 28K is ample to reconstruct tomograms having 64x64 = 4096 picture elements. The inverse matrices $G_{ij}(\underline{u})$ need to be pre-computed for a given geometry and number of planes and will reside on disk as a $\sim(N_p/2 + 1)^2$ x 4096 matrix. Calculation begins with the Fourier transforms of the N_p tomograms, one at a time, with rearrangement and storage on disc of the real and imaginary parts as a $(2N_p)$ x 4096 matrix. A given plane is reconstructed by bringing the T and G matrices into random access storage, a buffer-load at a time, and adding appropriate products of the elements of G and T into the real and imaginary parts of the 4096 object matrix. This requires $2N_p x 4096$ additions and multiplications. An inverse Fourier transform will give the reconstructed plane.

References

1. G.S. Freedman, Digital Gamma Camera Tomography-Theory, in Tomographic Imaging in Nuclear Medicine (Society of Nuclear Medicine, New York, 1973) G.S. Freedman, ed.), pg 68.

2. G. Muehllehner, Performance Parameters for a Tomographic Scintillation Camera, ibidem, pg 76

3. There are five different groups in this symposium reporting work with positron detectors. Figure 5 is modeled after that of D. Chu, et al, at Lawrence Berkeley Laboratory.

TECHNICAL INFORMATION DIVISION
LAWRENCE BERKELEY LABORATORY
UNIVERSITY OF CALIFORNIA
BERKELEY, CALIFORNIA 94720